

See discussions, stats, and author profiles for this publication at: <https://www.researchgate.net/publication/237163576>

# Catalysis by a Zinc–Porphyrin–Based Metal–Organic Framework: From Theory to Computational Design

DATASET · OCTOBER 2012

---

CITATION

1

---

READS

55

3 AUTHORS, INCLUDING:



Mark A. Ratner

Northwestern University


905 PUBLICATIONS 42,254 CITATIONS

SEE PROFILE

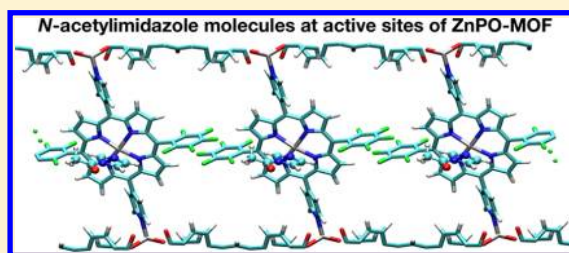
# Catalysis by a Zinc-Porphyrin-Based Metal–Organic Framework: From Theory to Computational Design

Sharani Roy,\* Christopher B. George,<sup>†</sup> and Mark A. Ratner

Department of Chemistry, Northwestern University, Evanston, Illinois 60208-3113, United States

 Supporting Information

**ABSTRACT:** Catalytic metal–organic frameworks (MOFs) have captured widespread attention for displaying shape, size, chemical, and enantiomeric selectivity characteristic of biological enzymes. Nguyen and co-workers [*J. Am. Chem. Soc.* **2009**, *131*, 4204–4205] synthesized a stable, crystalline, microporous, zinc-porphyrin-based metal–organic framework (ZnPO-MOF) that incorporates the catalytic activity of metalloporphyrins. They observed a 236-fold initial acceleration of an acyl-transfer reaction between 3-pyridylcarbinol and *N*-acetylimidazole by ZnPO-MOF, and attributed this catalysis primarily to a high local concentration or “preconcentration” of reactants at the porphyrin-Zn active sites of the framework. We report a detailed theoretical investigation of the framework-promoted reaction using the full atomic structure of the MOF. The three-step first-principles-based method developed for this purpose can be applied to study other catalytically active MOFs, and can help in the computational design of frameworks with optimum preconcentration and chemical sensing properties. Calculations show that reactants bind to the closely packed porphyrin-Zn sites of ZnPO-MOF, resulting in a high local concentration of catalyst-bound reactant. Our model predicts that reactant preconcentration in ZnPO-MOF can increase the initial rate of the acyl-transfer reaction by about 2 orders of magnitude relative to the uncatalyzed reaction, and can be the dominant catalytic mechanism in this system.



## 1. INTRODUCTION

Metal–organic frameworks (MOFs) have rapidly garnered tremendous interest due to their promising performance in a host of important applications, such as gas storage, gas separation, chemical sensing, and catalysis.<sup>2–16</sup> As the name suggests, MOFs are crystalline, porous materials comprised of an organic backbone anchored by metal ions, metal complexes, or metal-ion clusters. The structure and functionality of the organic ligands and the metal species, termed “secondary building blocks”, determine the dimensions of the pores as well as the reactivity of the MOF. By choosing suitable components, the chemical environment and pore size of a MOF can be designed to target specific molecules, e.g., they can selectively adsorb and separate a particular gas from a mixture of gases, such as CO<sub>2</sub> from CH<sub>4</sub> in natural gas.<sup>8</sup> While MOFs are reminiscent of the large surface areas and microporosity of zeolites, their structural diversity bestows very high versatility that cannot be achieved with the fully inorganic aluminosilicate structure of zeolites. While the organic components of MOFs compromise their stability at high temperatures, they create innumerable possibilities for structures with tailored properties. Explorations of such possibilities have expanded the repertoire of MOF applications to include drug delivery, electron and proton conduction, radiation detection, and light-emitting diodes.<sup>3,12</sup> Furthermore, this versatility is not limited to bulk MOF structures. Thin films and nanostructures of MOFs grown on substrates can function as smart membranes, catalytic coatings, and chemical sensors.<sup>17,18</sup>

Catalytically active MOFs permit constructing microenvironments with reactivities that are chemo-, size-, shape- and enantio-dependent.<sup>13–16,19–21</sup> The enormous chemical flexibility of MOF structures has permitted a diverse set of strategies for constructing such microenvironments, including MOF-encapsulated molecular or nanoparticle catalysts, catalysis at framework nodes, and the heterogenization of homogeneous catalysts within MOF struts.<sup>13</sup> The vast chemical space available for the design of MOF-based catalysts presents an opportunity for theoretical modeling to guide the development of materials with specific reactivities,<sup>22</sup> similar to the collaborative efforts that have proven fruitful in the design of MOFs with enhanced gas adsorption capabilities.<sup>9–11,23–25</sup> Steps toward the computational design of catalytically active MOFs have been taken in recent theoretical studies that utilized quantum mechanics and molecular mechanics to reveal mechanistic details of catalytic reactions in enantioselective MOFs.<sup>26,27</sup>

The present study is a theoretical investigation of catalysis by a zinc-porphyrin-based MOF.<sup>1</sup> By reacting Zn(NO<sub>3</sub>)<sub>2</sub>·6H<sub>2</sub>O with (5,15-dipyridyl-10,20-bis(pentafluorophenyl))porphyrin and 1,2,4,5-tetrakis(4-carboxylphenyl)benzene under solvothermal conditions, Shultz et al.<sup>1</sup> synthesized a crystalline, pillared paddlewheel MOF, shown in Figure 1. The crystal structure of this Zn-porphyrin “octa” MOF (ZnPO-MOF) revealed a catenation-free, three-dimensional framework with large,

Received: August 27, 2012

Published: October 2, 2012

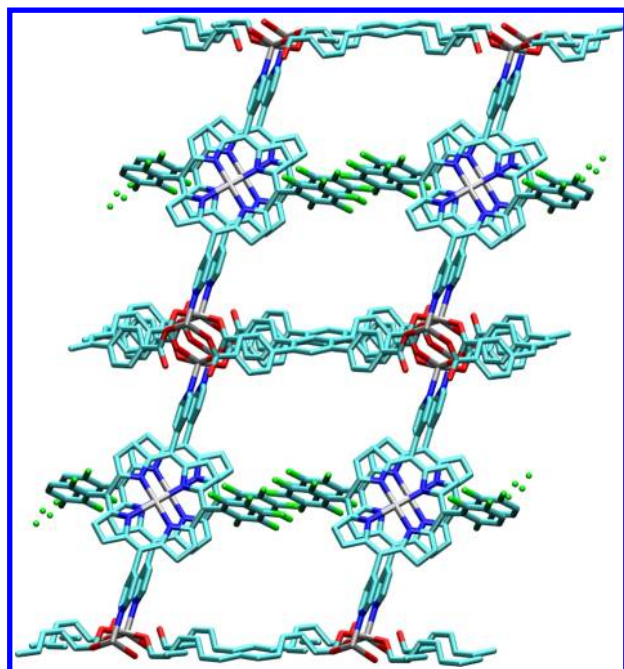
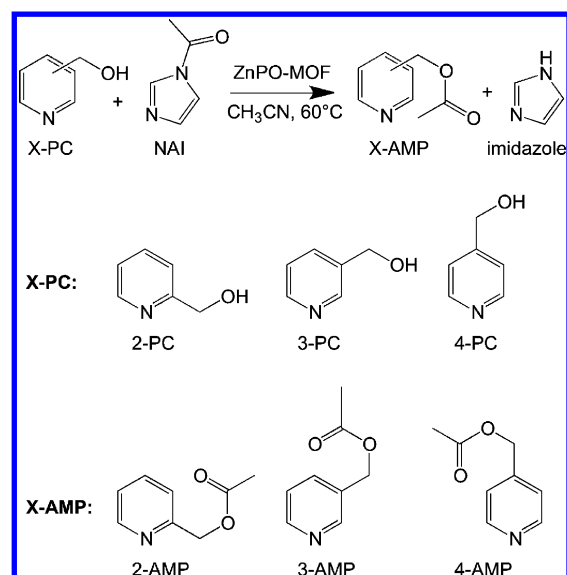


**Figure 1.** The periodic, three-dimensional structure of ZnPO-MOF, as synthesized by Shultz et al.<sup>1</sup> Color scheme for atoms: Zn = gray, F = green, O = red, N = blue, and C = cyan. H atoms are omitted for clarity.

solvent-occupied channels. The Zn atoms serve a dual purpose in this MOF. First, they anchor the substituted porphyrin rings to the tetratopic oxygen ligands, and second, they coordinate to the porphyrins during synthesis, forming metalloporphyrins. Characterization (powder X-ray diffraction, thermo-gravimetric analysis, reversible CO<sub>2</sub> adsorption isotherm, and NMR) confirmed that ZnPO-MOF fulfilled three important criteria for heterogeneous catalytic activity: robustness, permanent microporosity, and convenient access to active sites embedded in the cavities. An acyl-transfer reaction between 3-pyridylcarbinol (3-PC) and *N*-acetylimidazole (NAI) in the presence of ZnPO-MOF (Scheme 1) observed a 236-fold enhancement in the initial rate compared to the corresponding uncatalyzed reaction. The products were imidazole and 3-acetoxymethylpyridine (3-AMP). Acetonitrile (CH<sub>3</sub>CN) was used as solvent. The catalytic reaction was proposed to occur via binding of the reactants to the densely packed porphyrin-Zn sites inside the MOF, resulting in a high local concentration or “preconcentration”<sup>28</sup> of reactants. Experiments with ortho and para isomers of PC (Scheme 1) showed very similar catalytic rates for 2-PC and 3-PC, and a 2- to 3-fold lower rate for 4-PC. Based on these results, Shultz et al.<sup>1</sup> proposed that preconcentration was the major mechanism of catalysis because transition-state stabilization and favorable reactant alignment would be more sensitive to differences in isomer structures. They further supported this hypothesis by studying the preconcentration-free homogeneous catalysis of the acyl-transfer reaction by (tetraphenylporphyrin)Zn (ZnTPP), and observing an initial rate enhancement factor of slightly greater than 2.

This paper presents a three-step approach to calculate the catalytic rate enhancement of the acyl-transfer reaction due to preconcentration in ZnPO-MOF. The goal is to investigate the importance of reactant preconcentration in this system. The method also provides qualitative insight into transition-state

**Scheme 1.** The MOF-Catalyzed Acyl-Transfer Reaction between PC and NAI<sup>a</sup>



<sup>a</sup>The products are imidazole and AMP. The ortho (2-), meta (3-) and para (4-) isomers of PC and AMP are displayed below the reaction.

stabilization and reactant alignment by the MOF. In the first step, the binding characteristics of reactants, products and solvent at the porphyrin-Zn active site of ZnPO-MOF were calculated using density functional theory (DFT). In the second step, these results were used to compute temperature-dependent equilibrium constants for reactant binding and product dissociation at the catalytic sites. Finally, a kinetic model for heterogeneous MOF catalysis was devised, based on a mechanism similar to that proposed by Shultz et al.<sup>1</sup> This model was used to calculate the preconcentration component of the catalytic rate enhancement. This simple and efficient method is not limited to ZnPO-MOF, but rather can be used as a computational tool in tandem with experiments to examine and design catalytic MOFs with optimum preconcentration properties.

The remainder of the paper is organized as follows: Section 2 delineates the theoretical strategy. Section 3 presents the results and discussion on catalysis by ZnPO-MOF, and Section 4 presents a short study on the homogeneous catalysis of the acyl-transfer reaction by ZnTPP. Section 5 states some specific applications of the theoretical model, and finally, Section 6 summarizes the work and concludes with some suggestions to further enhance catalysis by ZnPO-MOF.

## 2. METHOD

This section describes the three-step method to calculate the preconcentration-based initial rate enhancement of the MOF-catalyzed reaction. In the first step (Section 2.1), DFT calculations were used to study the binding of reactants, products, and solvent to the active site of the MOF. In the second step (Section 2.2), the binding properties were used to calculate equilibrium constants for reactant binding and product dissociation at the active site. Finally, in the third step (Section 2.3), a rate expression was derived to calculate the preconcentration-based initial catalytic enhancement using the initial reactant concentrations, active-site concentration in the MOF, and the calculated reactant binding constants.

**2.1. DFT Calculations of Binding of Reactants, Products, and Solvent to MOF.** DFT calculations were performed using the Vienna Ab Initio Simulation Package (VASP, version 4.6.36),<sup>29</sup> a code that uses plane waves as the basis set. VASP imposes periodic boundary conditions on a given unit cell to model an infinite crystal, and is therefore ideal for studying ground-state properties of crystalline solids. The unit cell of ZnPO-MOF,<sup>1</sup> shown in Figure 2, has dimensions  $a$

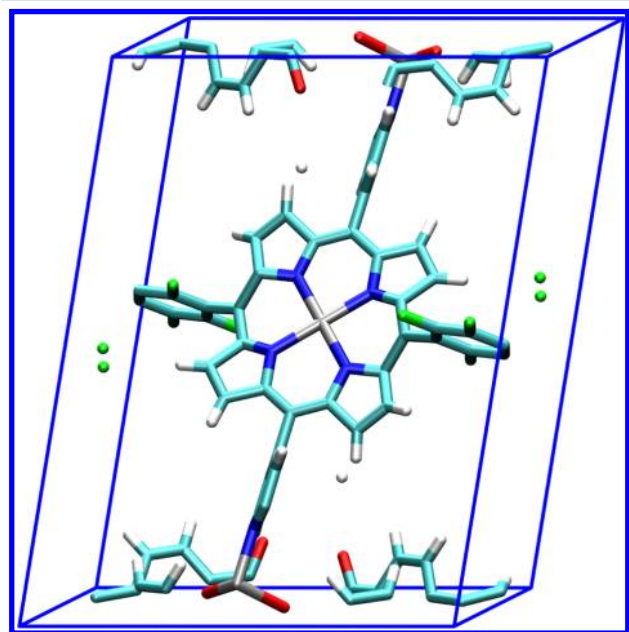


**Figure 2.** The unit cell of ZnPO-MOF.<sup>1</sup> Color scheme for atoms: Zn = gray, F = green, O = red, N = blue, C = cyan, and H = white.

$= 11.569 \text{ \AA}$ ,  $b = 15.447 \text{ \AA}$ ,  $c = 21.190 \text{ \AA}$ ,  $\alpha = 76.79^\circ$ ,  $\beta = 79.03^\circ$ , and  $\gamma = 89.61^\circ$ . It consists of 137 atoms, including 3 Zn atoms, 10 F atoms, 8 O atoms, 6 N atoms, 76 C atoms, and 34 H atoms.

Details of the calculations are presented here. The first Brillouin zone of the crystal was represented by one irreducible  $k$ -point. Exchange-correlation was described using the Perdew-Burke-Ernzerhof (PBE) functional<sup>30</sup> based on the generalized gradient approximation (GGA). Interactions between the nuclei and core electrons were described using the inbuilt projector-augmented-wave (PAW) pseudopotential<sup>31,32</sup> optimized for the PBE functional, leaving a total of 522 explicit valence electrons for ZnPO-MOF plus the valence electrons for the molecular species. The plane wave basis had an energy cutoff of 400 eV. Ground-state properties were determined from finite-temperature variational calculations using the Gaussian smearing method with a smearing width of 0.05 eV.<sup>33</sup>

The physical quantities calculated using DFT were the binding energies, binding geometries, and vibrational frequencies of reactant, product, and solvent molecules bound to the catalytic porphyrin-Zn sites of the MOF. Our model does not consider the attractive van der Waals interactions between the molecules and the entire MOF framework, which pull the molecules inside the MOF and are critical in studies of applications such as gas storage.<sup>11</sup> It focuses on reactant preconcentration specifically at the periodic active sites of the MOF, and the contribution of this preconcentration to catalysis. Details regarding calculation of these binding properties are provided in the Supporting Information.

**2.2. Equilibrium Constants for Reactant Binding and Product Dissociation.** Since the solvent, acetonitrile, has an electron-rich nitrogen environment like the reactants and products, the electropositive porphyrin-Zn atomic sites of the MOF are initially complexed by solvent molecules. Therefore, to achieve a catalytic acyl-transfer reaction, a reactant molecule must displace a solvent molecule to bind to an active site of the MOF:



where “MOF-solvent” and “MOF-reactant” respectively denote a solvent and reactant molecule bound to the porphyrin-Zn site of the MOF. The penta-coordinated  $\text{Zn}^{2+}$  ion is already bound to four N atoms of the porphyrin ligand (Figure 2), and can therefore bind to either one  $\text{CH}_3\text{CN}$  molecule, or one reactant molecule (NAI or PC). In a simple noninteracting model, the equilibrium constant for the displacement of a MOF-bound  $\text{CH}_3\text{CN}$  molecule by a NAI or PC molecule can be calculated from standard statistical thermodynamics. The total system is described by a canonical ensemble, and the equilibrium constant,  $K$ , for eq 1 is given by

$$K(T) = \frac{[\text{MOF-reactant}]}{[\text{MOF-solvent}][\text{reactant}]} = \frac{Q_{\text{MOF-reactant}} Q_{\text{solvent}}}{Q_{\text{MOF-solvent}} Q_{\text{reactant}}} \quad (2)$$

where  $K(T)$  is the temperature-dependent equilibrium constant,  $[\text{MOF-reactant}]$  is the concentration of reactant-bound porphyrin-Zn sites in the MOF,  $[\text{MOF-solvent}]$  is the concentration of solvent-bound porphyrin-Zn sites in the MOF, and  $[\text{reactant}]$  is the concentration of reactant in solution. Since the concentration of solvent can be assumed to be constant, it is set equal to 1 in accordance with concepts of heterogeneous equilibria. Therefore, it does not appear in the numerator of the first quotient. The four  $Q$ 's are the canonical partition functions for the respective species. These partition functions can be calculated using known constants and the DFT-derived physical quantities described in Section 2.1. The equations for the partition functions are presented in the Supporting Information.

Dissociation of products from the catalytic porphyrin-Zn sites of the MOF following the acyl-transfer reaction can be described similarly to eq 1. If the product molecules are not easily removed, they will block the active sites and inhibit further catalysis. Since reactant and product concentrations are low, displacement of product by solvent can be assumed to be the dominant method of product loss from the MOF. Within our model, product dissociation is the reverse of reactant binding:



The equilibrium constant for eq 3 was calculated similarly to  $K(T)$  for eq 1.

These reactant binding and product dissociation constants are derived from a simple model system of noninteracting reactant and solvent molecules. Since the reactant concentration is low, the interaction of one reactant molecule with another reactant molecule can be considered to be negligible. The reactant-solvent and solvent-solvent interactions are dominated by steric and dipole-dipole interactions, so they can be assumed to be relatively weak. Consequently, the model is considered to be a physically reasonable representation of the system. While the DFT calculations are not performed in the presence of a solvent environment, the important interaction of



a solvent molecule with the MOF catalytic site, and its effect on reactant or product binding is explicitly included. Solvation would be critical to stabilize the charged transition state relative to the reactants; however, this study does not calculate any transition states. It focuses on the thermodynamic preconcentration of reactants and dissociation of products at the MOF active sites.

**2.3. Kinetic Model of MOF-Catalyzed Reaction.** In this section, we examine the kinetics of the bimolecular reaction:



under three conditions: (a) uncatalyzed, (b) homogeneously catalyzed by metalloporphyrin molecules in solution, and (c) heterogeneously catalyzed by a crystalline MOF such as ZnPO-MOF with metalloporphyrin struts. The rate of the uncatalyzed reaction is given by

$$\text{Rate}_{\text{uncat}} = k_r[R1][R2] \quad (5)$$

where  $k_r$  is the bimolecular rate constant. When the reaction is homogeneously catalyzed by metalloporphyrins, the rate is given by

$$\text{Rate}_{\text{cat-homo}} = k'_r[R1-\text{Porphyrin}][R2] + k'_r[R1][R2-\text{Porphyrin}] \quad (6)$$

where R1-Porphyrin and R2-Porphyrin are the reactant-porphyrin complexes, and  $k'_r$  is the new bimolecular rate constant. Due to stabilization of the transition state by the metalloporphyrin,  $k'_r$  is greater than  $k_r$ . It is assumed for simplicity that  $k'_r$  is the same for R1 or R2 binding to the metalloporphyrin. Also, the term involving both catalyst-bound reactants is neglected because the catalyst concentration is much lower than reactant concentrations. The equilibrium concentrations of the reactant-porphyrin complexes are given by the coupled equations

$$K_{b1} = \frac{x}{([Porphyrin]_0 - x - y)([R1]_0 - x)} \quad (7)$$

and

$$K_{b2} = \frac{y}{([Porphyrin]_0 - x - y)([R2]_0 - y)} \quad (8)$$

where  $x = [R1-\text{Porphyrin}]$  and  $y = [R2-\text{Porphyrin}]$ .  $K_{b1}$  and  $K_{b2}$  are the binding constants of R1 and R2, respectively, to the metalloporphyrin, and the subscript "0" denotes initial condition. From eqs 5 and 6, the initial rate enhancement due to homogeneous catalysis is given by

$$\frac{\text{Rate}_{\text{cat-homo}}}{\text{Rate}_{\text{uncat}}} = \left( \frac{k'_r}{k_r} \right) \left\{ \frac{[R1-\text{Porphyrin}][R2]_0 + [R1]_0[R2-\text{Porphyrin}]}{[R1]_0[R2]_0} \right\} \quad (9)$$

where  $[R1-\text{Porphyrin}]$  and  $[R2-\text{Porphyrin}]$  can be calculated using eqs 7 and 8.

When the reaction is heterogeneously catalyzed by a crystalline MOF such as ZnPO-MOF with metalloporphyrin struts, the rate can be expressed similarly to eq 6:

$$\text{Rate}_{\text{cat-hetero}} = k'_r[R1-\text{Porphyrin}_{\text{MOF}}][R2] + k'_r[R1][R2-\text{Porphyrin}_{\text{MOF}}] \quad (10)$$

where  $[R1-\text{Porphyrin}_{\text{MOF}}]$  and  $[R2-\text{Porphyrin}_{\text{MOF}}]$  are the equilibrium concentrations of the reactant-porphyrin complexes inside the MOF. If the metalloporphyrin component of

the MOF is identical to the one used in homogeneous catalysis, then the rate constant can be assumed to be  $k'_r$ . Again, the catalyzed reaction mainly occurs between one bound reactant and one free reactant, because the distance between cofacial porphyrins is long enough that two neighboring bound reactants would either form a very unstable transition state or not react at all. Also, the probability is lower because neighboring bound reactants could be of the same species.  $[R1-\text{Porphyrin}_{\text{MOF}}]$  and  $[R2-\text{Porphyrin}_{\text{MOF}}]$  can be defined as

$$[R1-\text{Porphyrin}_{\text{MOF}}] = \theta_{R1}[Porphyrin_{\text{MOF}}]_0 \quad (11)$$

and

$$[R2-\text{Porphyrin}_{\text{MOF}}] = \theta_{R2}[Porphyrin_{\text{MOF}}]_0 \quad (12)$$

where  $\theta_{R1}$  and  $\theta_{R2}$  denote the reactant-bound fractions of the total metalloporphyrin concentration inside the MOF, expressed by  $[Porphyrin_{\text{MOF}}]_0$ . Since the amount of catalyst is small compared to the reactants, it is the limiting reagent and becomes saturated. In addition, since the reactant-porphyrin<sub>MOF</sub> equilibrium is heterogeneous, it can be assumed that solution concentrations of  $[R1]$  and  $[R2]$  change negligibly when the concentration of reactant-occupied porphyrin sites in the solid MOF changes. Therefore  $\theta_{R1}$  and  $\theta_{R2}$  are given by

$$\begin{aligned} \theta_{R1} &= [R1-\text{Porphyrin}_{\text{MOF}}] / \left( [Porphyrin_{\text{MOF}}] \right. \\ &\quad \left. + [R1-\text{Porphyrin}_{\text{MOF}}] + [R2-\text{Porphyrin}_{\text{MOF}}] \right) \\ &= \frac{K_{b1}}{1 + K_{b1} + K_{b2}} \end{aligned} \quad (13)$$

and

$$\theta_{R2} = \frac{K_{b2}}{1 + K_{b1} + K_{b2}} \quad (14)$$

From eqs 5 and 10–12, the initial enhancement due to heterogeneous catalysis is given by

$$\frac{\text{Rate}_{\text{cat-hetero}}}{\text{Rate}_{\text{uncat}}} = \left( \frac{k'_r}{k_r} \right) \left\{ \frac{\theta_{R1}[R2]_0 + \theta_{R2}[R1]_0}{[R1]_0[R2]_0} \right\} \frac{[Porphyrin_{\text{MOF}}]_0}{[Porphyrin_{\text{MOF}}]_0} \quad (15)$$

In eq 15, the initial concentration of a free reactant inside the MOF is assumed to be equal to the initial concentration of the reactant outside the MOF.

### 3. RESULTS AND DISCUSSION

**3.1. Binding of Reactants, Products, and Solvent to Active Site of ZnPO-MOF.** The reactants, NAI and PC, bind to the catalytic porphyrin-Zn site via their aromatic-N atoms, and the solvent, CH<sub>3</sub>CN, binds via its cyanide-N atom. The molecular plane (molecular axis for solvent) is oriented approximately perpendicular to the plane of the porphyrin ring, and the Zn atom exhibits 'doming', i.e., it protrudes out of the porphyrin plane to optimize the interaction with the molecule. The Zn atoms that act as connecting points between the substituted porphyrins and tetrapopic ligands of the MOF are already five-coordinated, so they do not compete with the porphyrin-Zn atoms for reactant or solvent binding. Calculations show that the Zn–O interaction is considerably weaker

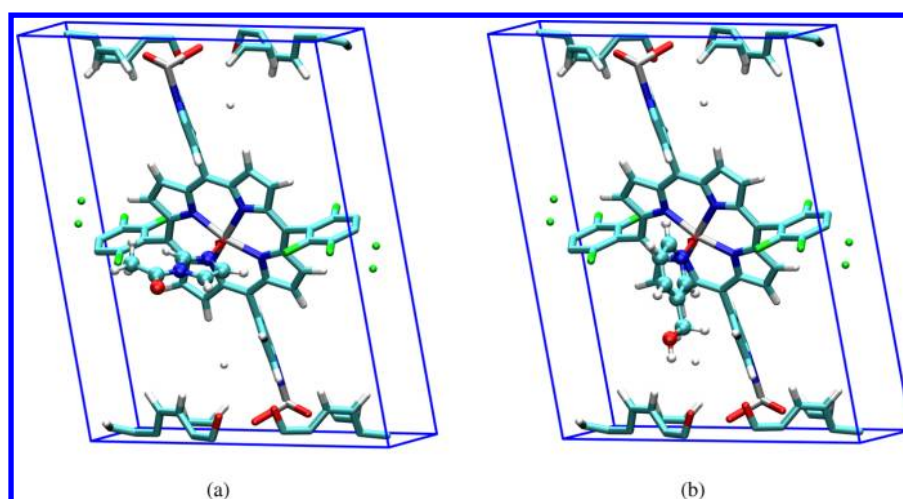


**Figure 3.** The DFT-optimized geometries of ZnPO-MOF-bound reactants (a) NAI and (b) 3-PC. Color scheme for atoms: Zn = gray, F = green, O = red, N = blue, C = cyan, and H = white. The reactants are shown in ball-and-stick representation to distinguish them from the MOF. The red arrow denotes the coordinate-covalent bond between the N atom of the reactant molecule and the porphyrinic Zn atom.

**Table 1. Binding Characteristics of the Reactants, NAI and Isomers of PC, and the Solvent, CH<sub>3</sub>CN, Bound to the Porphyrin-Zn Catalytic Site of (a) ZnPO-MOF, and (b) a Single, Isolated Porphyrin Fragment of ZnPO-MOF<sup>a</sup>**

solvent and reactants	ZnPO-MOF			substituted porphyrin monomer		
	$\Delta E_b$ (kcal/mol)	Zn–N distance (Å)	Zn doming (Å)	$\Delta E_b$ (kcal/mol)	Zn–N distance (Å)	Zn doming (Å)
CH <sub>3</sub> CN	6.4	2.28	0.26	6.0	2.28	0.24
NAI	12.4	2.18	0.32	11.6	2.20	0.32
2-PC	8.6	2.35	0.38	8.4	2.33	0.38
3-PC	14.1	2.21	0.33	11.2	2.21	0.33
4-PC	12.2	2.18	0.35	10.9	2.24	0.35

<sup>a</sup>The reported quantities are (a) the binding energy,  $\Delta E_b$ , (b) the Zn–N bond length between the porphyrinic Zn and the N atom of the molecule, and (c) the Zn doming distance out of the plane of the porphyrin ring.

than the Zn–N interaction, so NAI and PC prefer to bind via their aromatic-N atoms. Also, the reactants interact very weakly with the fluorinated phenyl substituents on the porphyrin ring. On the basis of these results, we conclude that the porphyrinic Zn atom is the most stable binding site for the reactants inside ZnPO-MOF. Figure 3 shows the DFT-optimized geometries for NAI and 3-PC, respectively, bound to the catalytic porphyrin-Zn site of ZnPO-MOF.

Table 1 shows the binding properties of reactant and solvent molecules at the catalytic porphyrin-Zn site of the MOF. While the binding energies of NAI, 3-PC, and 4-PC are very similar, the binding of 2-PC is compromised by steric repulsion between the porphyrin ring and the ortho substituent on the pyridine. The Zn–N distance varies between 2.2 and 2.3 Å for the reactants and the solvent, whereas the average distance between the Zn atom and each of the four porphyrin-N atoms (not shown in Table 1) varies between 2.05 and 2.1 Å. The Zn atom domes out of the porphyrin ring by 0.2–0.4 Å, with maximum doming for 2-PC to minimize steric repulsion. Table 1 also reports the same properties for each molecule bound to an isolated porphyrin-Zn fragment of the MOF. In these calculations, a Zn-coordinated (5,15-dipyridyl-10,20-bis-(pentafluorophenyl))porphyrin was placed inside a large  $20 \times 30 \times 30$  Å<sup>3</sup> unit cell to minimize interactions with replica images and model an isolated porphyrin. Binding energies and geometries of reactants and solvent are very similar to those inside the MOF, indicating that the architecture of the MOF does not affect the binding of these small molecules to the active sites.

Results for binding characteristics of product molecules at the catalytic porphyrin-Zn site are shown in Table 2. Overall,

**Table 2. Binding Characteristics of the Products, Imidazole and Isomers of AMP, Bound to the Porphyrin-Zn Catalytic Site of ZnPO-MOF<sup>a</sup>**

products	$\Delta E_b$ (kcal/mol)	Zn–N distance (Å)	Zn doming (Å)
imidazole	13.5	2.17	0.36
2-AMP	7.1	2.41	0.36
3-AMP	14.0	2.21	0.35
4-AMP	10.8	2.20	0.35

<sup>a</sup> $\Delta E_b$  is the binding energy, Zn–N distance is the distance between the porphyrin-Zn atom and the aromatic-N atom of the product, and Zn doming is the distance by which the Zn atom protrudes out of the plane of the porphyrin ring.

this binding behavior is similar to that of reactants. As expected, 2-AMP binds poorly due to unfavorable steric effects. The product molecules bind more strongly than solvent, suggesting that at high concentrations they might block the catalyst. The high binding energy of imidazole corroborates the experimental results of Shultz et al.<sup>1</sup> that demonstrate formidable product inhibition by imidazole. Figure 4 shows the DFT-optimized geometries for imidazole and 3-AMP, respectively, bound to the catalytic porphyrin-Zn site of ZnPO-MOF.

To summarize, the energetics show that the reactants can displace solvent molecules from the porphyrin-Zn site and preconcentrate at the MOF active sites. Product binding is

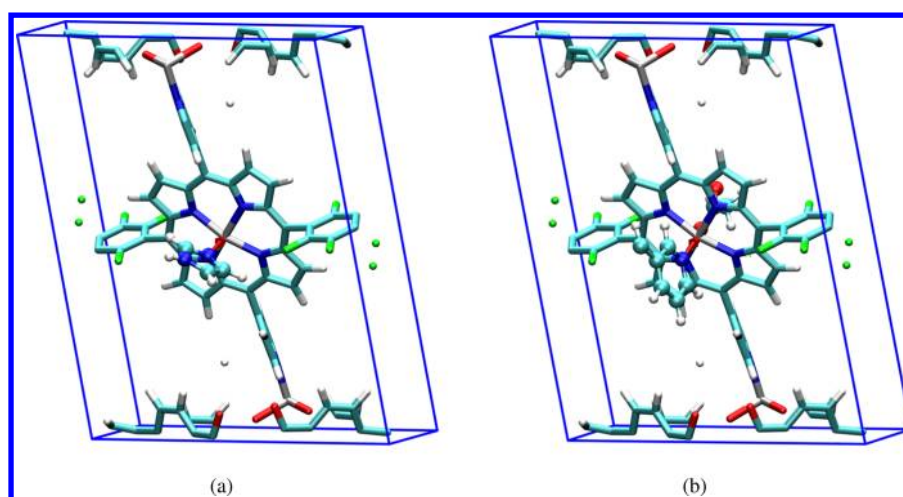


**Figure 4.** The DFT-optimized geometries of ZnPO-MOF-bound products, (a) imidazole and (b) 3-AMP. Color scheme for atoms: Zn = gray, F = green, O = red, N = blue, C = cyan, and H = white. The products are shown in ball-and-stick representation to distinguish them from the MOF. Part of the 3-AMP molecule is wrapped around to the back of the unit cell due to periodic boundary conditions. The red arrow denotes the coordinate-covalent bond between the N atom of the product molecule and the porphyrinic Zn atom.

similar to that of reactants, suggesting that product molecules, in particular imidazole and 3-AMP, can block catalytic sites at high concentrations. In addition to preconcentration, two important results on reactant alignment and orientation emerge from the minimum-energy structures. First, since each reactant binds via its aromatic-N atom, it is oriented favorably toward an approaching coreactant for an acyl-transfer reaction. Second, DFT calculations showed that the reactant binding energy is quite insensitive to rotation about the Zn–N axis. This conformational flexibility suggests that the structure of the MOF does not hinder the reactants from achieving an optimum transition state.

**3.2. Reactant Binding Constants and Product Dissociation Constants.** Table 3 presents the computed binding

**Table 3.** Binding Constants,  $K_b$ , of Reactants and Dissociation Constants,  $K_d$ , of Products at 60 °C<sup>a</sup>

$K_b$ of Reactants at 60 °C ( $M^{-1}$ )		$K_d$ of Products at 60 °C ( $M^{-1}$ )	
NAI	147	Imidazole	0.001
2-PC	0.2	2-AMP	30
3-PC	1906	3-AMP	0.0003
4-PC	76	4-AMP	0.5

<sup>a</sup>The reactants are NAI and the isomers of PC. The products are imidazole and the isomers of AMP.

constants of reactants at the reaction temperature of 60 °C used in experiments by Shultz et al.<sup>1</sup> The calculated equilibrium constants correspond to the binding of reactants to the catalytic porphyrin-Zn atom of the MOF, and are calculated as described in Section 2.2. Results show that 3-PC has the highest binding constant, whereas 2-PC has the lowest binding constant due to steric repulsion. These values show that NAI, 3-PC and 4-PC will effectively preconcentrate at the active sites of the MOF. Figure 5a plots the calculated reactant binding constants at four temperatures: 25 °C, 40 °C, 60 °C, and 80 °C. Our model can predict the temperature sensitivity of reactant binding, and can be used to tune the initial reaction temperature in order to enhance preconcentration. Table 3 also shows the product dissociation constants at 60 °C, while Figure 5b shows the variation of product binding constants with temperature. 2-

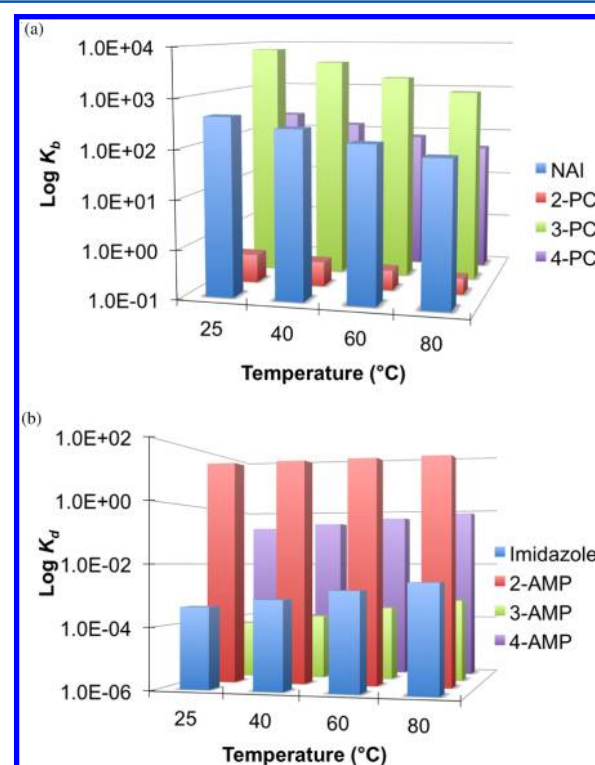


**Figure 5.** Temperature dependence of (a) reactant binding constant,  $K_b$ , for NAI and isomers of PC, and (b) product dissociation constant,  $K_d$ , for imidazole and isomers of AMP.

AMP dissociates much more easily than 3-AMP and 4-AMP. Imidazole has a low dissociation constant and consequently will be difficult to remove from the MOF active sites. Once again, this result agrees with the experimental result<sup>1</sup> that imidazole inhibits the catalyst at high concentrations. Increasing temperature can help to dissociate products and combat product inhibition.

**3.3. Catalytic Rate Enhancement due to Preconcentration.** The effect of reactant preconcentration on the catalytic rate in the MOF was calculated using the kinetic model presented in Section 2.3. The initial reactant



**Table 4.** Heterogeneous Catalysis of the Acyl Transfer Reaction between NAI and PC by 10 mol % of Crystalline ZnPO-MOF<sup>a</sup>

	$K_{\text{NAI}}$ ( $\text{M}^{-1}$ )	$K_{\text{PC}}$ ( $\text{M}^{-1}$ )	[X-Porphyrin] (mM)		[X-Porphyrin] <sub>MOF</sub> (mM)		Preconcentration-based enhancement factor
			X = NAI	X = PC	X = NAI	X = PC	
2-PC	147	0.2	0.598	0.002	795	1	133
3-PC	147	1906	0.031	0.569	57	745	92
4-PC	147	76	0.333	0.266	526	272	118

<sup>a</sup>[NAI]<sub>0</sub> = 6 mM, [PC]<sub>0</sub> = 9 mM, [Porphyrin]<sub>MOF</sub><sub>0</sub> = 0.802 M, and the reaction temperature is 60 °C. The binding constants,  $K_{\text{NAI}}$  and  $K_{\text{PC}}$  are calculated in Section 3.2. [NAI-Porphyrin]<sub>MOF</sub> and [PC-Porphyrin]<sub>MOF</sub> denote the equilibrium concentrations of the reactant-bound porphyrin-Zn sites inside the MOF. For a qualitative comparison with homogeneous catalysis, [NAI-Porphyrin] and [PC-Porphyrin] show the corresponding concentrations for a 10 mol % homogeneous solution (0.6 mM) of the same metalloporphyrin catalyst. The final column shows the preconcentration-based initial rate enhancement factor due to ZnPO-MOF catalysis.

concentrations of [NAI]<sub>0</sub> = 6 mM and [PC]<sub>0</sub> = 9 mM, and a reaction temperature of 60 °C were used in accordance with experimental conditions.<sup>1</sup> The solvent-accessible void volume of the ZnPO-MOF unit cell, as calculated by Shultz et al.<sup>1</sup> using the SQUEEZE program is 2069.6 Å<sup>3</sup>. Since there is one porphyrin per unit cell, the concentration of porphyrins in the MOF = [Porphyrin]<sub>MOF</sub><sub>0</sub> = 0.802 M. Therefore the binding of reactants to the porphyrins in the MOF creates very high local concentrations of porphyrin-bound reactants compared to the initial reactant concentrations, i.e., the MOF significantly preconcentrates the reactants. Table 4 shows the MOF-porphyrin-bound reactant concentrations, and compares them to the corresponding concentrations for a 10 mol % (0.6 mM) homogeneous solution of the same catalyst. Since the binding energies and geometries were found to be very similar for the MOF and its isolated porphyrin fragment (Section 3.1), the same binding constants were used for the heterogeneous and homogeneous cases. The catalyst-bound reactant concentrations inside the MOF are 2–3 orders of magnitude greater than the corresponding concentrations in homogeneous catalysis. On the basis of these enhanced local concentrations, the last column shows the initial rate enhancement due to reactant preconcentration in ZnPO-MOF. Results demonstrate that reactant preconcentration can independently increase the initial catalytic rate enhancement by up to 2 orders of magnitude, as proposed by Shultz et al.<sup>1</sup> A comparison of the experimentally observed total enhancement factor of 236 for 3-PC to the calculated preconcentration-based enhancement factor of 92 strongly suggests that preconcentration is the major component of the total rate enhancement in this system. In addition, the preconcentration factor is similar for all three isomers, just as the observed total rate enhancement is also similar for all the isomers. This agreement further indicates that preconcentration is the dominant catalytic mechanism in this system, since activation energies and collision frequencies would be more sensitive to structural variations in isomers.

#### 4. HOMOGENEOUS CATALYSIS BY ZNTPP

Shultz et al.<sup>1</sup> studied the homogeneous catalysis of the same acyl transfer reaction by a 10 mol % solution of ZnTPP, and observed an increase in the initial rate of the reaction by a factor of approximately 2. It is interesting to investigate whether this difference between a homogeneous catalytic enhancement factor of 2 by ZnTPP and a heterogeneous catalytic enhancement factor of 236 by ZnPO-MOF is primarily due to MOF preconcentration, or due to significant differences in transition-state stabilization by the two catalysts. Table 5 shows the binding properties of the solvent and reactants to the Zn center of ZnTPP. Calculations were performed by placing a single ZnTPP molecule inside a 20 × 30 × 30 Å<sup>3</sup> unit cell,

**Table 5.** Binding Characteristics of the Reactants, NAI and PC, and the Solvent, CH<sub>3</sub>CN, Bound to the Zn Atom of ZnTPP<sup>a</sup>

solvent and reactants	$\Delta E_b$ (kcal/mol)	Zn–N distance (Å)	Zn doming (Å)	$K_b$ at 60 °C ( $\text{M}^{-1}$ )
CH <sub>3</sub> CN	3.1	2.34	0.21	
NAI	8.6	2.23	0.29	70
2-PC	5.2	2.39	0.33	0.2
3-PC	9.1	2.23	0.30	936
4-PC	7.6	2.33	0.34	11

<sup>a</sup> $\Delta E_b$  is the Binding energy, Zn–N distance is the distance between the porphyrin-Zn atom and the aromatic-N atom of the reactant or solvent, Zn doming is the distance by which the Zn atom protrudes out of the plane of the porphyrin ring, and  $K_b$  is the active-site binding constant.

similar to the study of reactant binding to isolated ((5,15-dipyridyl-10,20-bis(pentafluorophenyl))porphyrin)Zn in Section 3.1. The binding energies and, consequently, the binding constants of reactants are weaker with ZnTPP than with ZnPO-MOF. This difference can be attributed to the electron-withdrawing pentafluorophenyl and pyridyl substituents on the porphyrin ring in ZnPO-MOF, which render the Zn more electropositive and a stronger Lewis acid. A weaker bond between the reactants and ZnTPP suggests less stabilization of the charged transition state for acyl transfer. While the incorporation of ZnTPP in a heterogeneous environment can significantly increase the initial catalytic enhancement via preconcentration, as demonstrated in Section 3.3 for ZnPO-MOF, the transition state is also more stabilized by the substituted porphyrin in ZnPO-MOF.

DFT calculations of reactant and solvent binding to ZnTPP can be compared to previous experimental studies of ZnTPP complexes. Szintay and Horvath<sup>34</sup> measured the absorption and fluorescence emission spectra of various ZnTPP complexes in toluene at temperatures ranging between 20 and 60 °C, and used them to derive the thermodynamic parameters for the porphyrin-ligand interactions. They determined  $\Delta H$  for binding of acetonitrile to ZnTPP to be equal to 6.8 kcal/mol, and that for isomers of pyridine derivative, picoline to be equal to 8.0 kcal/mol (2-picoline), 9.3 kcal/mol (3-picoline), and 10.3 kcal/mol (4-picoline). These values are in good qualitative agreement with our results. Also, the porphyrin-molecule Zn–N bond lengths, porphyrin Zn–N distances, and Zn doming distances in crystal structures of ZnTPP–picoline and ZnPP–acetonitrile complexes reported by Gomila et al.<sup>35</sup> are in good agreement with our calculated geometries. Furthermore, our simple noninteracting model yields a binding constant of 189 M<sup>−1</sup> for NAI-ZnTPP at 25 °C, which is about a factor of 4 from the corresponding experimental value of 801 M<sup>−1</sup>



determined by Shultz et al.<sup>1</sup> using UV–vis titrations. Figure 6 shows the DFT-optimized geometries of reactants, NAI and 3-PC, bound to the Zn atom of ZnTPP.

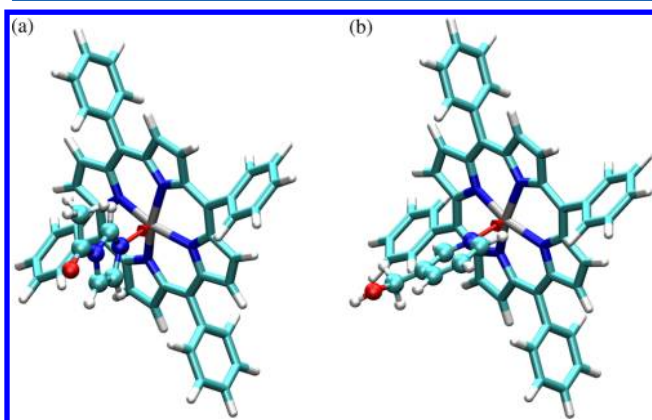


**Figure 6.** The DFT-optimized geometries of ZnTPP-bound reactants, (a) NAI and (b) 3-PC. Color scheme for atoms: Zn = gray, F = green, O = red, N = blue, C = cyan, and H = white. The reactants are shown in ball-and-stick representation to distinguish them from the MOF. The red arrow denotes the coordinate-covalent bond between the N atom of the reactant molecule and the Zn atom of ZnTPP.

## 5. APPLICATIONS OF THEORETICAL MODEL

The three-step theoretical model of MOF catalysis proposed in this work can be used to examine active-site preconcentration in different MOFs and to design catalytic MOFs with optimal preconcentration properties. Here are some specific applications of our model.

1. The model can be used to calculate binding constants of reactants and dissociation constants of products at the active site of a MOF. The binding constants will reveal how effectively the reactants will preconcentrate and which reactants will preconcentrate more. The dissociation constants will reveal which products will cause serious inhibition of catalysis as product concentrations increase. If the active-site environment of the MOF or the shape and size of MOF channels is unfavorable for the reactants under consideration, our periodic model will capture the problem in the form of low binding constants. This method for calculating molecular binding constants can also be applied to design MOFs for sensing small target molecules.
2. The model can be used to study the temperature dependence of reactant binding constants and product dissociation constants in order to choose optimum temperatures for the catalytic reaction. Low temperatures can help to increase reactant preconcentration, while high temperatures can help to curb product inhibition.
3. The kinetic model presented in Section 2.3 can be used to predict the maximum initial rate enhancement obtainable from preconcentration for a given MOF structure, known initial reactant concentrations, and calculated active-site reactant binding constants. Therefore, this model can be used to tune these parameters in order to optimize reactant preconcentration. Specifically, this model can aid in the design of MOF architectures that maximize the concentration of active sites without sterically hindering reactant binding.

## 6. SUMMARY AND CONCLUSIONS

Shultz et al.<sup>1</sup> synthesized ZnPO-MOF, a robust, microporous, three-dimensional MOF with Zn-coordinated porphyrin struts. They studied its catalytic activity and observed that it enhanced the initial rate of an acyl-transfer reaction between NAI and 3-PC by a factor of 236. This prolific catalysis was primarily attributed to the increased local concentration or preconcentration of reactants at the catalytic porphyrin-Zn sites of the framework. We calculate binding and dissociation constants of reactants and products at the active site of the MOF using DFT calculations and equilibrium statistical mechanics. Using a simple kinetic model, we calculate the preconcentration-based initial catalytic enhancement of the acyl-transfer reaction using the calculated reactant binding constants, initial reactant concentrations, and the active-site concentration in the MOF. This theoretical model is not limited to ZnPO-MOF and can be used to study active-site preconcentration in different catalytic MOFs, or to design catalytic MOFs with optimum preconcentration properties. Results show that reactant preconcentration in ZnPO-MOF can boost the initial catalytic rate enhancement by up to 2 orders of magnitude. Our calculated preconcentration-based enhancement factor of 92 for NAI+3-PC compared to the observed total enhancement factor of 236 strongly suggests that reactant preconcentration is the dominant catalytic mechanism in this system. Our results also qualitatively reproduce other experimental results such as product inhibition by imidazole. On the basis of this study, we offer three suggestions to further improve catalysis by ZnPO-MOF. First, preconcentration and product inhibition could be tuned by changing the reaction temperature. Lowering the temperature could increase reactant preconcentration, and increasing the temperature periodically could decrease product inhibition. Second, a flow reactor could be used to maintain a constant flux of reactants in order to curb product inhibition. Finally, a different metal atom instead of Zn might stabilize the transition state more effectively, as well as increase preconcentration.

## ■ ASSOCIATED CONTENT

### § Supporting Information

(1) Details of calculations of binding energy, binding geometry, and vibrational frequencies of a molecule bound to a porphyrin-Zn active site of ZnPO-MOF. (2) Expressions for total partition functions of a free molecule and a MOF-bound molecule, including expressions for translational, rotational, vibrational, and electronic partition functions. This material is available free of charge via the Internet at <http://pubs.acs.org/>.

## ■ AUTHOR INFORMATION

### Corresponding Author

\*E-mail: [sharani-roy@northwestern.edu](mailto:sharani-roy@northwestern.edu).

### Present Address

<sup>†</sup>Intel Corporation, Hillsboro, OR 97124

### Notes

The authors declare no competing financial interest.

## ■ ACKNOWLEDGMENTS

We are very grateful to the Multidisciplinary University Research Initiative (MURI) (Grant Number: FA9550-07-1-0534) from the Air Force Office of Scientific Research (AFOSR) for their support. C.B.G. thanks the NSF for his graduate fellowship. We thank the research groups of Joseph Hupp and SonBinh Nguyen for an exciting collaboration, and

especially thank Abraham Shultz for detailed discussions. S.R. thanks John Tully, Abraham Nitzan, Henry Heitzer, Alan True, and Shashank Shekhar for insightful discussions.

## REFERENCES

- (1) Shultz, A. M.; Farha, O. K.; Hupp, J. T.; Nguyen, S. T. *J. Am. Chem. Soc.* **2009**, *131*, 4204–4205.
- (2) Yaghi, O. M.; Li, G.; Li, H. *Nature* **1995**, *378*, 703–706.
- (3) Meek, S. T.; Greathouse, J. A.; Allendorf, M. D. *Adv. Mater.* **2011**, *23*, 249–267.
- (4) Murray, L. J.; Dincă, M.; Long, J. R. *Chem. Soc. Rev.* **2009**, *38*, 1294–1314.
- (5) Murray, L. J.; Dinca, M.; Yano, J.; Chavan, S.; Bordiga, S.; Brown, C. M.; Long, J. R. *J. Am. Chem. Soc.* **2010**, *132*, 7856–7857.
- (6) Keskin, S. J. *Phys. Chem. C* **2011**, *115*, 800–807.
- (7) Watanabe, T.; Sholl, D. S. *J. Chem. Phys.* **2010**, *133*, 094509.
- (8) Li, J.-R.; Kuppler, R. J.; Zhou, H.-C. *Chem. Soc. Rev.* **2009**, *38*, 1477–1504.
- (9) Babarao, R.; Eddaoudi, M.; Jiang, J. W. *Langmuir* **2010**, *26*, 11196–11203.
- (10) Keskin, S.; Liu, J.; Rankin, R. B.; Johnson, J. K.; Sholl, D. S. *Ind. Eng. Chem. Res.* **2009**, *48*, 2355–2371.
- (11) Düren, T.; Bae, Y.-S.; Snurr, R. Q. *Chem. Soc. Rev.* **2009**, *38*, 1237–1247.
- (12) Allendorf, M. D.; Bauer, C. A.; Bhakta, R. K.; Houk, R. J. T. *Chem. Soc. Rev.* **2009**, *38*, 1330–1352.
- (13) Lee, J.; Farha, O. K.; Roberts, J.; Scheidt, K. A.; Nguyen, S. T.; Hupp, J. T. *Chem. Soc. Rev.* **2009**, *38*, 1450–1459.
- (14) Lillerud, K. P.; Olsbye, U.; Tilset, M. *Top. Catal.* **2010**, *53*, 859–868.
- (15) Lin, W. *Top. Catal.* **2010**, *53*, 869–875.
- (16) Ma, L.; Abney, C.; Lin, W. *Chem. Soc. Rev.* **2009**, *38*, 1248–1256.
- (17) Zacher, D.; Schmid, R.; Wöll, C.; Fischer, R. A. *Angew. Chem., Int. Ed. Engl.* **2011**, *50*, 176–99.
- (18) Zacher, D.; Shekhah, O.; Wöll, C.; Fischer, R. A. *Chem. Soc. Rev.* **2009**, *38*, 1418–29.
- (19) Ma, L.; Falkowski, J. M.; Abney, C.; Lin, W. *Nat. Chem.* **2010**, *2*, 838–46.
- (20) Wang, C.; Zheng, M.; Lin, W. *J. Phys. Chem. Lett.* **2011**, *2*, 1701–1709.
- (21) Cho, S.-H.; Ma, B.; Nguyen, S. T.; Hupp, J. T.; Albrecht-Schmitt, T. E. *Chem. Commun.* **2006**, 2563–2565.
- (22) Chizallet, C.; Lazare, S.; Bazer-Bachi, D.; Bonnier, F.; Lecocq, V.; Soyer, E.; Quoineaud, A.-A.; Bats, N. *J. Am. Chem. Soc.* **2010**, *132*, 12365–12377.
- (23) Liu, D.; Zhong, C. J. *Mater. Chem.* **2010**, *20*, 10308–10318.
- (24) Farrusseng, D.; Daniel, C.; Gaudillère, C.; Ravon, U.; Schuurman, Y.; Mirotatos, C.; Dubbeldam, D.; Frost, H.; Snurr, R. Q. *Langmuir* **2009**, *25*, 7383–7388.
- (25) Srepusharawoot, P.; Araújo, C. M.; Blomqvist, A.; Scheicher, R. H.; Ahuja, R. *J. Chem. Phys.* **2008**, *129*, 164104.
- (26) Oxford, G. A. E.; Dubbeldam, D.; Broadbelt, L. J.; Snurr, R. Q. *J. Mol. Catal. A: Chem.* **2011**, *334*, 89–97.
- (27) Oxford, G. A. E.; Snurr, R. Q.; Broadbelt, L. J. *Ind. Eng. Chem. Res.* **2010**, *49*, 10965–10973.
- (28) Ni, Z.; Jerrell, J. P.; Cadwallader, K. R.; Masel, R. I. *Anal. Chem.* **2007**, *79*, 1290–1293.
- (29) (a) Kresse, G.; Hafner, J. *Phys. Rev. B* **1993**, *47*, 558–561.  
(b) Kresse, G.; Furthmüller, J. *Comput. Mater. Sci.* **1996**, *6*, 15–50.  
(c) Kresse, G.; Furthmüller, J. *Phys. Rev. B* **1996**, *54*, 11169–11186.
- (30) Paier, J.; Hirschl, R.; Marsman, M.; Kresse, G. *J. Chem. Phys.* **2005**, *122*, 234102.
- (31) Blöchl, P. E. *Phys. Rev. B* **1994**, *50*, 17953–17979.
- (32) Kresse, G.; Joubert, D. *Phys. Rev. B* **1999**, *59*, 1758–1775.
- (33) Mermin, N. D. *Phys. Rev.* **1965**, *137*, A1441–A1443.
- (34) Szintay, G.; Horvath, A. *Inorg. Chim. Acta* **2000**, *310*, 175–182.
- (35) Gomila, R. M.; Quinonero, D.; Frontera, A.; Ballester, P.; Deya, P. M. *J. Mol. Struct. (THEOCHEM)* **2000**, *531*, 381–386.